KSTLE International Journal, Vol. 5, No. 2, December 2004, pp. 44-48

A FEM Analysis of Dynamic Behavior for a Slider with Curvature Effect

Sung Keun Lim and Yoon Chul Rhim*,†

Graduate School, Yonsei University
**School of Mechanical Engineering, Yonsei University*

Abstract: A new type slider with optical components is going to be introduced on market for portable and high capacity disk drive, and it will show a great potential for high performance drive in the near future. It is very important for a slider to have excellent dynamic characteristics regardless its physical size. In this paper the dynamic behavior and static characteristics of slider for a small form factor optical disk drive have been investigated numerically by an in-house simulation code using FEM. A curvature effect is found when a slider is applied to a relatively small disk, which makes rolling characteristics worse due to the negative pressure generated at the air bearing surface because of the curvature of small disk diameter.

Keywords: Curvature effect, modified reynolds equation, dynamic behavior of a slider, FEM

Introduction

These days, personal computers become indispensable to everyone's life. It is not unusual that one has PC at the office as well as at home and sometimes one even needs additional mobile PC. Using these PCs, people exchange various kinds of information through the network or removable media. . The average amount of information handled per day per person is already over 10 MB and it increases rapidly with contents of information and technology development of storage device. People now want to have a small portable I/O device to retrieve the data as the most hand-held personal electronic devices converge to one ubiquitous system. Therefore a small form factored information storage device is required to satisfy these requirements. An optical disk drive (ODD) has better characteristics than a hard disk drive (HDD) from the points of view of distribution of data and contamination of the media. A swing arm type ODD is developed to increase the data transfer rate. It has a slider which has to fly over the rotating media with optical component. A load/unload system for the slider is also adopted both to save data zone and to keep removability. A suitable air bearing surface (ABS) can bear applied static as well as dynamic load during the slider is loading and flying.[1-3].

In this study we are going to focus on the curvature effect which arises when the radius of disk is relatively small compared to the width of a slider. It is common to use linear velocity of the disk to compute the dynamic characteristics of a slider. However, curvature effect must be considered when small diameter disk is used or the slider is located in inner diameter position. Static and dynamic characteristics of an optical slider are computed with in-house simulation code based on FEM[4] and dynamic equations of motion.

†Corresponding author: Tel: 82-2-2123-2820, Fax: 82-2-312-2159
E-mail: rhimyc@yonsei.ac.kr

Numerical Model

Air Bearing

A slider is one of applications of self-acting gas lubricated bearings. A non-dimensionalized modified Reynolds equation is used to analyze the air bearing between the slider and the rotating disk. Since the air gap is very thin, 2nd order slip effect should be considered in terms of flow factor, Q_p, as suggested in Fukui-Kaneko model[5].

$$\frac{\partial}{\partial X}\left(PH^3Q_p\frac{\partial P}{\partial X}\right)+\lambda^2\frac{\partial}{\partial Y}\left(PH^3Q_p\frac{\partial P}{\partial Y}\right) = \Lambda_X\frac{\partial PH}{\partial X}+\Lambda_Y\frac{\partial PH}{\partial Y}+\sigma\frac{\partial PH}{\partial T} \quad (1)$$

Since the air flow under the slider is due to the rotating disk, the curvature as well as the slider position in radial direction must be considered in the governing equation as shown in Fig. 1. The modified Reynolds equation is recast as follows:

$$\frac{\partial}{\partial X}\left(PH^3Q_p\frac{\partial P}{\partial X}\right)+\lambda^2\frac{\partial}{\partial Y}\left(PH^3Q_p\frac{\partial P}{\partial Y}\right) = \Lambda_X\frac{\partial PH}{\partial X}+\Lambda_Y\frac{\partial PH}{\partial Y}+\sigma\frac{\partial PH}{\partial T}+\alpha PH\frac{\partial U^*}{\partial X}+\beta PH\frac{\partial V^*}{\partial Y} \quad (2)$$

The boundary conditions for Eqn. (2) are obvious. The pressure normalized with ambient pressure at four sides is set to unity, i.e.,

$$P = 1 \text{ along } X = 0,\ X = 1,\ Y = 0, \text{ and } Y = 1 \quad (3)$$

In order to obtain the pressure distribution in thin air film, weighted residual method is applied to the Eqn. (2). The residual for Eqn. (2) is defined as follows.

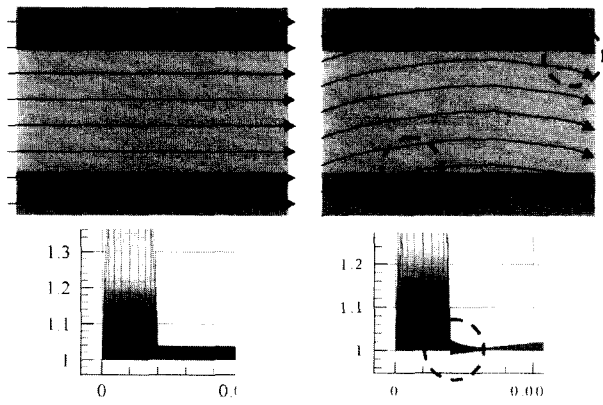

Fig. 1. Comparison of linearized and actual velocity field under the two-rail slider.

$$R(p) = \frac{\partial}{\partial X}\left(PH^3Q_p\frac{\partial P}{\partial X}\right) + \lambda^2\frac{\partial}{\partial Y}\left(PH^3Q_p\frac{\partial P}{\partial Y}\right) - \Lambda_X\frac{\partial PH}{\partial X} - \Lambda_Y\frac{\partial PH}{\partial Y} - \sigma\frac{\partial PH}{\partial T} - \alpha PH\frac{\partial U^*}{\partial X} - \beta PH\frac{\partial V^*}{\partial Y} \quad (4)$$

Let [N] be a suitable weighting function in the weak formulation process. After multiplying Eqn. (4) by [N] as follows:

$$W(p) = \int_\Lambda [N]^T[R(P)]dA = \int_\Lambda [N]^T \begin{bmatrix} \frac{\partial}{\partial X}\left(PH^3Q_p\frac{\partial P}{\partial X}\right) + \lambda^2\frac{\partial}{\partial Y}\left(PH^3Q_p\frac{\partial P}{\partial Y}\right) \\ -\Lambda_X\frac{\partial PH}{\partial X} - \Lambda_Y\frac{\partial PH}{\partial Y} - \sigma\frac{\partial PH}{\partial T} \\ -\alpha PH\frac{\partial U^*}{\partial X} - \beta PH\frac{\partial V^*}{\partial Y} \end{bmatrix} dA \quad (5)$$

where [N] is the row vector containing the element shape functions according to Bubnov-Galerkin's method.

Integrating by parts over a sub-domain, employing the Green-Gauss Theorem, and applying boundary conditions given in Eqn. (3), Eqn. (5) becomes

$$W(p) = -\int_\Lambda \begin{bmatrix} PH^3Q_p\left(\frac{\partial N}{\partial X}\frac{\partial P}{\partial X} + \lambda^2\frac{\partial N}{\partial Y}\frac{\partial P}{\partial Y}\right) \\ -PH\left(\Lambda_X\frac{\partial N}{\partial X} + \Lambda_Y\frac{\partial N}{\partial Y}\right) \\ +N\sigma P\frac{\partial H}{\partial T} + N\sigma H\frac{\Delta(P-P^{n-1})}{\Delta t} \\ -\alpha PHU^*\frac{\partial N}{\partial X} - \beta PHV^*\frac{\partial N}{\partial Y}dA \end{bmatrix} \quad (6)$$

Newton-Raphson iteration procedure can be employed to solve a nonlinear integro-differential Eqn. (6). Beginning with an initial guess for $P^{(0)}$, Newton-Raphson method may be used to construct a sequence $P^{(1)}$, $P^{(2)}$, $P^{(3)}$, $\cdots$, defined as follows:

$$P^{(n+1)} = P^{(n)} + \Psi^{(n)} \quad (7)$$

where $\psi^{(n)}$ is a solution of the linear problem.

$$W'(P^{(n)})\Psi^{(n)} + W(P^{(n)})\Psi^{(n)} = 0 \quad (8)$$

In Eqn. (8), $W'(P^{(n)})$ is the Frechet derivative of $W(P^{(n)})$ with respect to P evaluated at $P = P^{(n)}$. If it exists, this linear operator is defined by

$$W'(P^{(n)})\Psi^{(n)} = \lim_{\varepsilon\to 0}(W(P^{(n)} + \varepsilon\Psi^{(n)})) = 0 \quad (9)$$

Using Eqns. (8) and (9), Eqn. (6) may be written as

$$[\mathbf{K}_1 - \mathbf{K}_2 + \mathbf{K}_3]\Psi^{(n)} = [F_1 + F_2] \quad (10)$$

where,

$$[\mathbf{K}_1] = \int_\Lambda PH^3Q_p\left[\frac{\partial N}{\partial X}\frac{\partial N}{\partial X} + \lambda^2\frac{\partial N}{\partial Y}\frac{\partial N}{\partial Y}\right] + [N]H^3Q_p\left[\frac{\partial N}{\partial X}\frac{\partial P}{\partial X} + \lambda^2\frac{\partial N}{\partial Y}\frac{\partial P}{\partial Y}\right]dA$$

$$[\mathbf{K}_2] = \int_\Lambda H\left[\Lambda_X\frac{\partial N}{\partial X} + \Lambda_Y\frac{\partial N}{\partial Y}\right][N]dA$$

$$[\mathbf{K}_3] = \int_\Lambda \frac{NN\sigma H}{\Delta T} + NN\sigma\frac{\partial H}{\partial T}dA$$

$$[\mathbf{F}_1] = -\int_\Lambda PH^3Q_p\left[\frac{\partial P}{\partial X}\frac{\partial N}{\partial X} + \lambda^2\frac{\partial P}{\partial Y}\frac{\partial N}{\partial Y}\right] - PH\left[\Lambda_X\frac{\partial P}{\partial X} + \Lambda_y\frac{\partial N}{\partial Y}\right]dA$$

$$[\mathbf{F}_2] = -\int_\Lambda \left(\alpha U^*\frac{\partial N}{\partial X} + \beta V^*\frac{\partial N}{\partial Y} + \frac{N\sigma H}{\Delta T} + N\sigma P\frac{\partial H}{\partial T} - \frac{\sigma H}{\Delta T}NP^{n-1}\right)dA$$

The convergence criterion used for the Newton-Raphson iteration is

$$\frac{\sum|P^{n+1} - P^n|}{\sum|P^{n+1}|} \le k \quad (11)$$

where k is adequately small.

Under-relaxation is used to fasten the convergence and to stabilize the iteration like the following manner:

$$P^{(n+1)} = P^{(n)} + a(\Psi^{(n)}) \quad 0 \le a \le 1 \quad (12)$$

where a is an under-relaxation factor.

Mapping

The quadrilateral element is used in this study. Mapping and derivatives of the shape function with respect to x and y coordinates can be calculated as

$$\frac{\partial N}{\partial \xi} = \frac{\partial N}{\partial x}\frac{\partial x}{\partial \xi} + \frac{\partial N}{\partial y}\frac{\partial y}{\partial \xi}$$

$$\frac{\partial N}{\partial \eta} = \frac{\partial N}{\partial x}\frac{\partial x}{\partial \eta} + \frac{\partial N}{\partial y}\frac{\partial y}{\partial \eta}$$

$$\begin{pmatrix} \frac{\partial N}{\partial \xi} \\ \frac{\partial N}{\partial \eta} \end{pmatrix} = \begin{pmatrix} \frac{\partial x}{\partial \xi}\frac{\partial y}{\partial \xi} \\ \frac{\partial x}{\partial \eta}\frac{\partial y}{\partial \eta} \end{pmatrix} \begin{pmatrix} \frac{\partial N}{\partial x} \\ \frac{\partial N}{\partial y} \end{pmatrix} = J \begin{pmatrix} \frac{\partial N}{\partial x} \\ \frac{\partial N}{\partial y} \end{pmatrix} \tag{13}$$

Since element matrix and vector are given in x,y coordinates system in general cases, we must replace equations with ξ, η coordinates system.

$$d\xi' = \begin{pmatrix} \frac{\partial x}{\partial \xi} \\ \frac{\partial y}{\partial \xi} \end{pmatrix} d\xi \quad d\eta' = \begin{pmatrix} \frac{\partial x}{\partial \eta} \\ \frac{\partial y}{\partial \eta} \end{pmatrix} d\eta$$

$$dA = |d\xi' \times d\eta'| = \left| \begin{pmatrix} \frac{\partial x}{\partial \xi} \\ \frac{\partial y}{\partial \xi} \end{pmatrix} \times \begin{pmatrix} \frac{\partial x}{\partial \eta} \\ \frac{\partial y}{\partial \eta} \end{pmatrix} \right| d\xi d\eta \tag{14}$$

$$dA = \begin{vmatrix} \frac{\partial x}{\partial \xi} & \frac{\partial y}{\partial \xi} \\ \frac{\partial x}{\partial \eta} & \frac{\partial y}{\partial \eta} \end{vmatrix} d\xi d\eta = |J| d\xi d\eta$$

Hence, two-dimensional integration in general x, y coordinates system is replaced with Eqn. (15).

$$\iint f(x, y)dxdy = \int_{-1}^{1}\int_{-1}^{1} g(\xi, \eta)|det[J]|d\xi d\eta \tag{15}$$

Slider Dynamics

Dynamic equations must be computed with modified Reynolds equation, simultaneously. Modified Reynolds equation is solved using in-house simulation code based on FEM and dynamic equations are solved using 4th-order Runge-Kutta algorithm. Pressure distribution from the solution of the modified Reynolds equation is used as a forcing function in system of dynamic equations and then new position of a slider can be obtained as a solution. New position of a slider generates a different pressure field and the computation iterates until the pre-set time is reached.

A slider is attached to a suspension through a flexure and preload is applied to the dimple point at the slider. Even though the slider has six degrees of freedom, we are interested in three major motions such as pitching, rolling, and z-direction motion, as shown in Fig. 2. Three major motions can be expressed by following dynamic equations:

$$M\frac{\partial^2 Z}{\partial t^2} + C_Z\frac{\partial Z}{\partial t} + K_Z Z = \int_\Lambda (P - P_a)dxdy - F_0$$

$$I_\theta\frac{\partial^2 \theta}{\partial t^2} + C_\theta\frac{\partial \theta}{\partial t} + K_\theta \theta = \int_\Lambda (P - P_a)(X - X_a)dxdy - F_0(X - X_a) \tag{16}$$

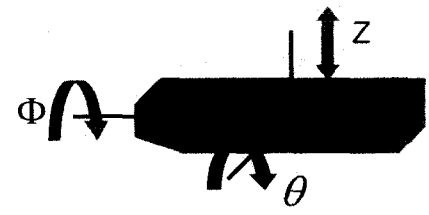

Fig. 2. Three degrees of freedom slider.

$$I_\Phi\frac{\partial^2 \Phi}{\partial t^2} + C_\Phi\frac{\partial \Phi}{\partial t} + K_\Phi \Phi = \int_\Lambda (P - P_a)(Y - Y_a)dxdy - F_0(Y - Y_a)$$

The suspension is modeled as a spring/damper system. In Eqn. (16), variables Z, θ, and Φ represent the vertical displacement at the slider's mass center, and the slider's pitching and rolling angles, respectively. Parameters M, I_θ, and I_Φ represent the mass and moments of inertia of the slider and K_θ, K_Φ, C_θ and C_Φ represent the stiffness and damping coefficients of the suspension in the pitching and rolling directions. F_0 is the preload applied to the slider by the suspension in Z-direction, P_a is the ambient pressure, and P is the pressure governed by the modified Reynolds equation.

As mentioned above, Dynamic equations are solved by 4th-order Runge-Kutta algorithm. For example, vertical direction equation proceeds as follows.

$$m\frac{\partial^2 z}{\partial t^2} + C_z\frac{\partial z}{\partial t} + K_z z = \int_\Lambda (P - P_a)dxdy - F_0$$

$$v = \frac{\partial z}{\partial t} = f_2(t, v, z)$$

$$\frac{\partial v}{\partial t} = \frac{1}{m}\int_\Lambda (p - p_a)dxdy - \frac{F_0}{m} - \frac{C_z}{m}v - \frac{K_z}{m}z = f_1(t, v, z) \tag{17}$$

$$v_{i+1} = v_i + \frac{1}{6}(k_{1.1} + 2k_{2.1} + 2k_{3.1} + k_{4.1})\Delta t$$

$$z_{i+1} = z_i + \frac{1}{6}(l_{1.1} + 2l_{2.1} + 2l_{3.1} + l_{4.1})\Delta t$$

Figure 3 shows the flow chart of the simulation. First, guess initial values for the slider position and motion, then the modified Reynolds equation and system of dynamic equations are solved iteratively.

Computational Results

Static Results

The flying height of the slider varies as the head is moved from the inner radius (ID) to the outer radius (OD) of the disk in disk drives with rotary actuators. The flying height is determined from the combined effect of the disk velocity and the skew angle which change as the slider moves from ID to OD.

A tri-pad slider is used to evaluate the static results. Figure 4

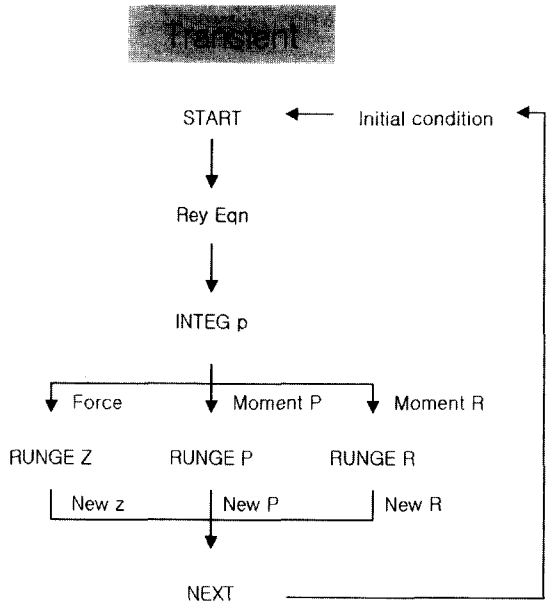

Fig. 3. Flow chart of simulation.

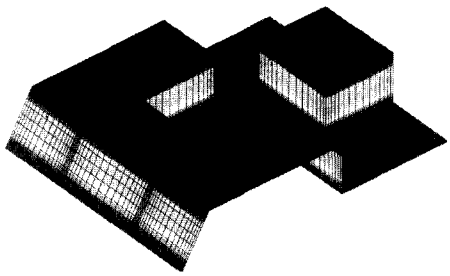

Fig. 4. Air bearing surface of the tri-pad slider.

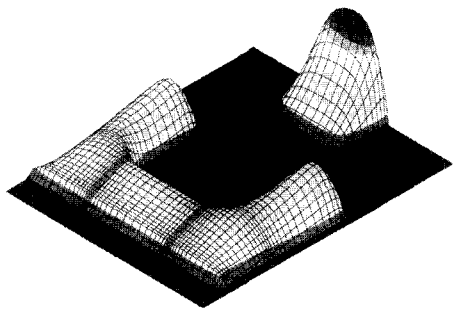

Fig. 5. pressure distribution of tri-pad slider.

shows the ABS of the slider and Fig. 5 shows the typical pressure distribution over the ABS. The pressure distribution shows some difference when the velocity is assumed linear and when the actual velocity distribution is applied to the calculation. We can see this difference clearly in two-rail slider as shown in the Fig. 1. We can even observe negative pressure generated due to the curvature effect and the slider dynamics affected by this pressure distribution.

Figure 6 shows differences of the static characteristics of tri-pad slider between linear velocity and real velocity distribution. Pitching and rolling angle do not vary much for

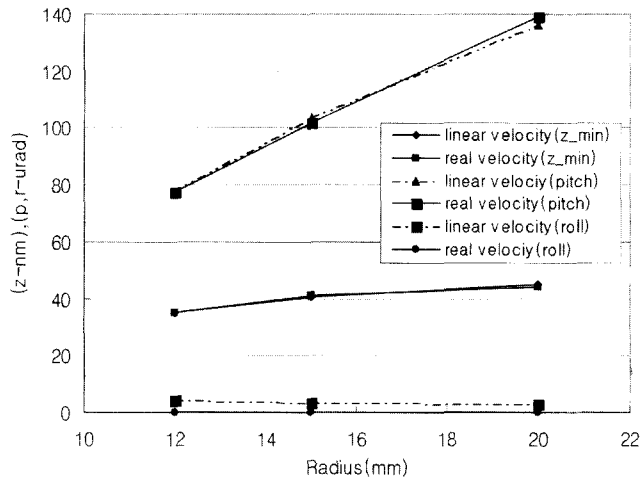

Fig. 6. Comparison of the static characteristics for linearized and real velocity field.

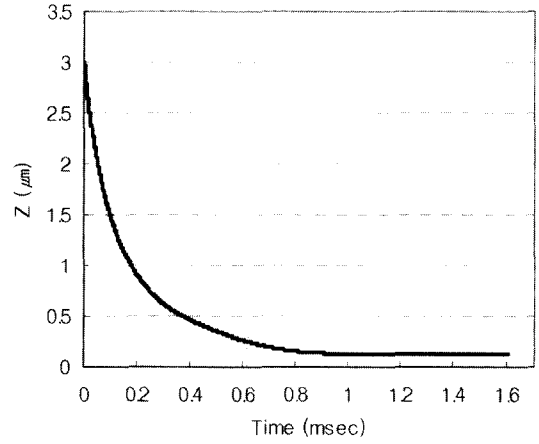

Fig. 7. Vertical displacement variation of the slider during the falling from 3 mm above the disk.

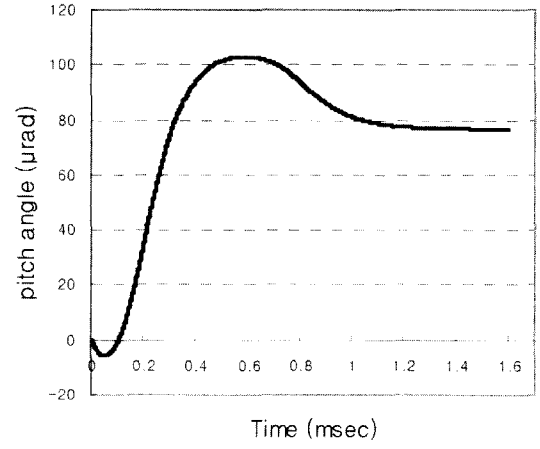

Fig. 8. Pitching angle variation of the slider during dynamic simulation.

the velocity distribution but the flying height is reduced less than half.

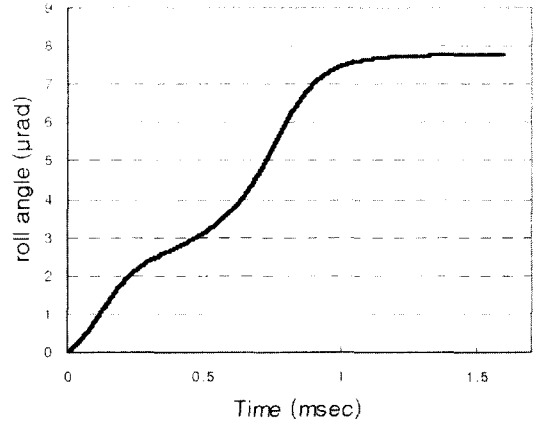

Fig. 9. Rolling angle variation of the slider during dynamic simulation.

Dynamic Results

Transient simulation for the motion of tri-pad slider is performed using dynamic equations and modified Reynolds equation. The slider falls from its initial position of 3 mm above the disk, the initial falling velocity is zero, initial pitching and rolling angles are set to 0 mrad. Figures 7, 8, and 9 show z-height variations, pitching angle, and rolling angle variations of the slider with respect to time.

If the velocity between slider and disk is assumed linear, rolling angle must be zero during the loading process because the ABS is symmetric to the center line of the slider so is the pressure distribution symmetric. However, as mentioned in the static results, rolling angle is not zero even in symmetric ABS is used for the actual velocity distribution is applied to the simulation.

Conclusion

Static characteristics and dynamic behavior of a slider are investigated by numerical simulation.

Comparisons of linearized and actual velocity field between slider and disk are investigated numerically and we can draw conclusion as follows:

1. Actual velocity distribution has less loading carrying capacity so that the flying height is smaller than linear velocity case.
2. Actual velocity distribution generate asymmetric pressure distribution so that the slider rolls during the loading process.
3. Pitching angle varies much while the slider moves from ID to OD due to linear velocity as well as skew angle and this variation affects the flying height.

Acknowledgment

This work was supported by the Grant No. R11-1997-042-12002-0 of CISD designated by KOSEF.

References

1. Ono, K., "Dynamic Characteristics of Air-Lubricated Slider Bearing for Noncontact Magnetic Recording," ASME J. of Tribology, Vol. 97, pp. 250-260, 1975.
2. White, M., 1983, "Flying Characteristics of the "Zero-Load" Slider Bearing," ASME J. of Lubrication Technology, Vol. 105, pp. 484-490.
3. Jeong T. G and Bogy, D., "Numerical Simulation of Dynamic Loading in Hard Disk Drives." ASME J. of Tribology, Vol. 115, NO. 3, pp. 370-375, 1993.
4. Peng, j.-p., and Haedie, C. E., 1995, "A Finite Element Scheme for Determining the Shaped Rail Slider Flying Characteristics with Experimental Confirmation," ASME J. of Tribology, Vol. 117, pp. 358-364.
5. Fukui, S., and Kaneko, R., "A database of Interpolation of Poiseuille Flow Rates for High Knudsen Number Lubrication Problems," ASME J. of Tribology, Vol. 112, pp. 78-83, 1990.

Nomenclature

P : dimensionless pressure; p/p_a
H : dimensionless clearance; h/h_{min}
X, Y : dimensionless coordinates; X=x/l, Y=y/b
T : dimensionless time; T=wt
L_X : bearing number; $6\mu Ul/ p_a h_{min}^2$
L_Y : bearing number; $6\mu Ul^2/ p_a b h_{min}^2$
s : squeeze number: $12\mu\omega l^2/p_a h_{min}^2$
Q_p : flow factor in slip flow model
U^* : dimensionless velocity; U/U_0
V^* : dimensionless velocity; V/V_0
α : $6\mu lU_0/ p_a h_{min}^2$
β : $6\mu l^2V_0/ p_a b h_{min}^2$
p_a : ambient pressure
h_{min} : minimum film thickness
l : slider length
b : slider width
U : x direction velocity
V : y direction velocity
U_0 : x direction standard velocity
V_0 : y direction standard velocity
ω : angular velocity
μ : viscosity